WILEY-VCH

DOI: 10.1002/ ((please add manuscript number))
Article type: Full Paper

Single-Shot Laser Additive Manufacturing of High Fill-Factor Microlens Arrays

*Salvatore Surdo, Riccardo Carzino, Alberto Diaspro, and Martí Duocastella**

Dr. S. Surdo, Dr. R. Carzino, Prof. A. Diaspro, Dr. M. Duocastella
Nanophysics, Istituto Italiano di Tecnologia, Via Morego 30, 16163, Genova, Italy
E-mail: marti.duocastella@iit.it

Keywords: miniaturized optics, LIFT, laser additive manufacturing, polymer patterning, resist reflow

High fill-factor microlens arrays (MLA) are key for improving photon collection efficiency in light-sensitive devices. Although several techniques are now capable of producing high-quality MLA, they can be limited in fill-factor, precision, the range of suitable substrates, or the possibility to generate arbitrary arrays. Here, a novel additive direct-write method for rapid and customized fabrication of high fill-factor MLA over a variety of substrates is demonstrated. This approach uses a single laser pulse to delaminate and catapult a polymeric microdisc from a film onto a substrate of interest. Following a thermal reflow process, the printed disc can be converted into a planoconvex microlens offering excellent sphericity and high smoothness (R_{RMS} <40A). Importantly, the transfer of solid microdiscs enables fill-factors close to 100%, not achievable with standard direct-write methods such as ink-jet printing or microdispensing. Arbitrary generation of MLA over flexible and curved surfaces, with microlenses presenting a curvature ranging from 20 to 240 µm and diffraction-limited performance are demonstrated. The ease of implementation and versatility of the approach, combined with its potential parallelization, paves the way for the high-throughput fabrication of tailored MLA directly on top of functional devices.

1. Introduction

The ability to fabricate customized microlens arrays (MLA) over user-selectable surfaces allows for the improved performance of optoelectronic systems.[1–4] Examples include the 2.6-fold increase in light extraction efficiency for organic-light-emitting diodes,[1] the ~10% enhancement of light absorption in polymeric solar cells,[2] or the possibility to reach pixel throughputs as high as 4Mpx/s in fluorescence microscopy.[3] While the potential of MLA as vehicles for enhancing photon collection efficiency is clear, the current challenge is to develop cost-effective technologies that enable rapid generation of tailored MLA directly on functional devices and with a high fill-factor (FF).[5,6] This latter, defined as the ratio of the area of the MLA covered by microlenses to its total area, directly correlates with the amount of light that the array can collect. Therefore, it is paramount to have technologies capable of generating MLA with a FF as high as possible, ideally 100%.

Various methods have been adopted for the high-FF fabrication of MLA. Hexagonal arrays with 100% FF have been demonstrated by self-assembly methods based on dewetting,[7] localized water condensation,[8] or surface wrinkling,[9] but these approaches typically lack control in the design and positioning of the microlenses. In contrast, photolithography techniques have become the gold standard for the production of customized high-FF MLA.[10–13] Even if unrivaled industrial upscaling is possible, photolithography is optimized for planar substrates and requires multistep processing in expensive clean room facilities. More importantly, the need of masks imposes an additional limit in the degree of tunability of the MLA designs in timely fashion.

Alternatively, direct-write technologies (DWTs) such as ink-jet printing,[14] microdispensing,[15] two-photon polymerization,[16] laser-induced forward transfer (LIFT),[17,18] or multibeam interference based holography,[19] enable the direct and maskless fabrication of polymeric microlenses and MLA with perfectly optical quality on a variety of

substrates. In this case, though, the use of liquid prepolymers can result in merging of adjacent microlenses that seriously constraint the attainable FF of the arrays.[20] Recent works to improve the FF using DWTs include the fabrication of concave MLA using laser ablation followed by a replica molding step.[21,22] Despite excellent results in terms of uniformity and FF, this approach impedes the direct fabrication of MLA on substrates of interest. Furthermore, most DWTs require complex systems or ultrafast lasers for parallelization, which limits the overall throughput of these systems. Simply put, a low-cost and maskless technique capable of directly generating high-FF arrays at high-throughputs, with controlled geometry and at targeted positions on non-planar substrates does not exist.

In this work, we present a novel laser-based method for the realization of high-FF polymeric microlens arrays that addresses the limitations of traditional direct-write and photolithographic approaches. Our method, termed laser catapulting or LCP, exploits short (in the nanosecond scale) high-energy laser pulses to transfer polymeric solid microdiscs from a uniform film into targeted positions on a receiver substrate. After thermal reflow, namely the heating of the microdiscs above their glass transition temperature (Tg), planoconvex microlenses are obtained. Notably, the direct printing of discs in the solid-state enables the generation of highly close-packed structures at high rates, which could not be achieved with liquid-based DWTs. Thus, LCP combines the benefits of direct-write methods in terms of design versatility, with the natural advantages of photolithography for the generation of high-FF MLA. We demonstrate our approach by fabricating and characterizing the morphology and optical properties of high-FF (up to 99%) arrays of tailored polymeric microlenses with excellent sphericity and smoothness over planar, flexible and curved substrates.

2. Results and discussion

The typical setup for a LCP experiment is shown in **Figure 1a**. In analogy to LIFT,[23–25] a pulsed laser source is directed to a polymer film, named donor, supported on a carrier

substrate transparent to the laser radiation. A second substrate, facing the donor and in close proximity to it, receives and collects the ejected material from the polymer film. Both substrates are placed on an XYZ translation stage and can move jointly relative to the laser beam. Thus, the simple firing of laser pulses at different donor positions enables the generation of arbitrary patterns of microdiscs. Following the printing process, the microdiscs are converted into planoconvex microlenses by thermal reflow. This step can be performed using a uniform heat source such as an oven or a hotplate, but it can also be implemented with laser sources. This latter allows local control of the reflow conditions and thus tuning of the optical properties for each individual microlens of the array. Note that a CMOS camera can be used for the direct visual inspection of the receiver substrate and controlled catapulting of discs at targeted positions. This represents a competitive advantage compared to traditional methods such as inkjet and photolithography, where either the nozzle or the mask hides the receiver substrate.

Figure 1b shows a schematic representation of the mechanisms that lead to delamination and catapulting of microdiscs. An in-depth analysis of the ejection dynamics of polymers by laser pulses have been reported in the context of LIFT,[26–28] with results readily applicable to the present case. In short, the arrival of a single laser pulse at the donor, provided a sufficiently high laser fluence, induces the generation of a gas-pocket at the donor-carrier substrate interface. Further expansion of the gas progressively increases the stress at the edges of the laser-irradiated region. When the ultimate stress of the polymer is exceeded, mechanical rupture of the polymer occurs and a microdisc is detached, which is then propelled to the receiver. Importantly, two main requirements are necessary to transfer a solid microdisc with LCP. First, laser absorption must be high enough to induce the formation of the gas-pocket and the delamination of the polymer. Second, the highest stresses have to be located at the edges of the delaminated region for proper disc formation. Otherwise, inhomogeneous film rupture is expected.[29] This condition is verified if the bending stresses

dominate over the stretching ones. In other words, the donor must be capable of resisting deformations during disc deflection. With the previous points in mind, the ideal donor must have a high absorbance in the laser wavelength, high Young modulus (>2 GPa) and low ultimate strength (<100 MPa). Examples of potential donors for LCP include thermoplastics (e.g. poly-methyl-methacrylate and polypropylene) and thermoset plastics (e.g. epoxy). In the current experiments, we used a spin-coated layer of S1813 as the donor, with a thickness between 2 and 10 μm. S1813 is a positive photoresist commonly used in photolithography, with high optical absorbance at λ=248 nm, high transparency in the visible, a Young modulus of 8 GPa and an ultimate strength of about 50 MPa.

Initially, we validated the feasibility of LCP for the fabrication of high-FF MLA on flat substrates. To this end, we prepared arrays of microdiscs on top of glass, a paradigmatic example of a rigid substrate, as well as on the elastomer polydimethylsiloxane (PDMS). Polymeric microdiscs printed on glass and PDMS at a fluence of 0.85 J/cm^2 are shown in Figure S1a and Figure 1c, respectively. In all cases, microdiscs are highly uniform with approximately the same size. Interestingly, stylus profilometry data (Figure S2) reveals that they do not exhibit a cylindrical shape, but rather that of a conical frustum. In particular, microdiscs display an upper region of 18 μm in agreement with the laser spot-size, together with a significantly larger base of ~70 μm. This shape can be attributed to the delamination process induced by the laser, which results in tilted fractures originating at the periphery of the deflected disc. Thus, the extent of the base widening depends on the distance that the fracture has to travel before crossing the entire disc thickness, as supported by experiments using a thinner donor. Such widening ultimately limits the minimum lens diameter that can be fabricated with the technique. Importantly, though, this deviation from the cylindrical shape does not preclude the use of LCP for the fabrication of microlenses. In fact, after reflow, the microdisc arrays are successfully converted into highly smooth planoconvex microlenses as reflected in Figure S1b and Figure 1d. Further morphological characterization by atomic force

microscopy (AFM) shows a lens surface roughness of only R_{RMS}=36A and a good sphericity (Figure 1e). This high quality is due to the action of surface tension that enables almost perfectly smooth and spherical surfaces.[30] Notably, even if no significant differences can be found between MLA fabricated on glass and on PDMS, the use of elastic and soft substrates facilitates the successful printing of microdiscs. Indeed, elastomers damp the kinetic energy of the microdisc and prevent its fracture during impact with the receiver substrate, which widens the processing window of LCP.

LCP comes with a large experimental parameter space that enables customized MLA fabrication based on application. Figure 2 shows different examples of the possibilities offered by LCP in terms of FF, microlens size, and receiver substrate. Notably, arrays with a fill-factor as high as 99% can be fabricated by LCP (Figure 2a). Control of the diameter of the microlenses of the MLA can be achieved by simply adjusting the laser spot size (Figure 2b). At conditions reported herein, microlenses with a diameter ranging from 20 to 130 µm could be fabricated by varying the laser spot size and donor film thickness (Figure S5). Interestingly, the microlenses of different size can be closely spaced without merging. Finally, MLA or individual microlenses can be generated on bendable substrates (Figure 2c) or directly on curved surfaces (Figure 2d). In the first case, we performed LCP on a PDMS substrate before bending. Instead, for the preparation of microlenses on top of a curved surface, we limited the catapulting process to the region where the distance between donor film and receiver substrate was of only some microns, which we controlled by optical inspection. Ideally, though, one could use a bendable donor film that conformally adopts to the shape of the receiver substrate in order to cover larger areas. Importantly, in all cases, the high optical quality, fill-factor, and uniformity of the fabricated structures are preserved. These results demonstrate the suitability of LCP for the fabrication of high-FF arrays with control in size and position at the single microlens level. In addition, it renders LCP compatible with novel optoelectronic systems

such as eye-compound cameras,[31] flexible displays[32] and solar cells[33] that require non-planar, elastic or flexible substrates.

To understand the remarkably high-FF values of LCP, we performed a more in-depth analysis of the dependency of this parameter on the distance between microdiscs and the geometry of the array (Figure 3). Thus, for a rectangular array, the maximum FF is 93%, whereas for a closely spaced array it is 99%. These high-FF values are above the theoretically predicted ones considering circular discs, which correspond to $\pi/4 \sim 78\,\%$ and $\pi/2\sqrt{3} \sim 91\,\%$ for the respective geometries. We attribute these unexpectedly high FF to two factors. First, the particular transfer mechanisms of LCP yield to microdiscs with a shape that is determined by both laser spot and available material in the irradiated area of the donor. Thus, the firing of two spatially adjacent laser pulses will not lead to two overlapping microdiscs, but rather to two interlocking structures with virtually no gap in-between. Second, the generated microdiscs do not merge during the reflow step. This is caused by the dominance of the resist cross-linking timescale over the viscous timescale at high temperatures (T>Tg), as observed from differential scanning calorimetry data (Figure S3). Further details on this phenomenon are provided in the Supporting Information. Note a key difference between LCP and photolithography. Whereas the latter requires chemical or physical boundaries to avoid merging of closely packed resist microcylinders and obtain high-FF MLA with high curvature,[11,12] LCP can achieve so by simply reflowing the laser-patterned resist. This is a clear advantage in terms of cost, efficiency and speed of the fabrication process.

Critical technological parameters for LCP are precision, accuracy, and radius of curvature (ROC) of the microlenses. Experimental determination of these quantities is summarized in Figure 4. The accuracy of LCP, calculated as the standard deviation of the measured centroid positions of each individual structure with respect to the expected ones, is 2 µm and 3 µm before and after reflow, respectively (Figure 4b). These values ultimately

depend on the resolution of the mechanical XY stage used in current experiments (±1 µm), and thus a higher accuracy is expected with a higher resolution stage. As shown in Figure 4c, the precision of LCP, namely the standard deviation of the diameter of the fabricated structures, presents a value of 0.2 µm for microdiscs (1% of disc diameter) and 0.4 µm for microlenses (0.6% of the lens diameter). The origin of such high precision is due to the stability of the laser source, the uniformity of the donor film and the pinning of the contact area between the disc and the substrate (Figure S3a), which enables to maintain the sub-micrometeric precision even after the reflow process. Importantly, pinning of the contact line, which comes naturally in LCP due to the possibility to decouple the wettability between receiver substrate and donor film, is typically difficult to achieve in photolithography.[34] LCP also offers control of the ROC of the fabricated microlenses by adjusting the laser spot size. In conditions herein (10 µm thick donor film), a ROC from 79 ± 3 µm to 242 ± 9 µm was obtained for spot diameters between 20 and 70 µm (Figure 4d). The upper limit in ROC is due to bulging of the microdisc. In this case, cross-linking occurs before the microdisc can reach a spherical shape. Instead, the lower limit of the ROC is given by the smallest feature size that can be catapulted. This size depends in turn on the ratio between the laser spot size and the donor film thickness. As expected from plate bending theory,[35] below a certain laser spot size and for a given film thickness, the donor is effectively so stiff that catapulting cannot occur at the laser fluences available in our system. This is confirmed by the lower ROC, down to ~24 µm, that can be achieved with a 2 µm thick donor film (Figure S4). From the values of ROC and considering the diameter of the microlenses, it is possible to calculate their focal length (f_S) and numerical aperture (NA). In current experiments, the respective values range from 48 to 480 µm, and from 0.13 to 0.24, as summarized in Table S1.

To test the focusing capabilities of the microlenses, we measured the point-spread function (PSF) and light collection efficiency of a MLA with a fill-factor of ~ 100%. Figure 5a shows the 3D-reconstructed PSFs of more than 100 nominally identical microlenses

measured by confocal microscopy. Notably, the microlenses present an excellent optical performance, with an average lateral PSF value of 2 ± 0.5 µm in agreement with the diffraction-limited PSF of ~ 1.8 µm (Figure 5b-c). The confocal images also show a signal-to-noise ratio of 30:1 between focused light and light from the array dead area. This is an indication of the high photon collection efficiency (η_{MLA}) of the MLA. A further quantification of this parameter as a function of the array FF is presented in Figure 5d. In this case, we calculated η_{MLA} as the ratio between the total number of photons collected by the microlenses to the photons illuminating the array. Note that η_{MLA} increases with the array fill-factor, from 56% for a FF of 68% to above 84% for a FF of 98%. Importantly, the relationship between η_{MLA} and FF is approximately linear, in agreement with the equation $\eta_{MLA} = \eta_{lens} \cdot FF$, where η_{lens} is the collection efficiency of an individual microlens. Thus, for a given FF, η_{lens} ultimately determines the overall performance of the MLA. This value depends on the NA of the microlens as well as on its optical aberrations. To characterize this latter, we used wavefront sensing and Zernike analysis (Figure 5e). As expected, defocus (related to the lens focusing power) is the main contribute to the Zernike polynomials, whereas high order aberrations are not significant. Additionally, we characterized chromatic aberrations by imaging through a MLA three circular dots with the same size, each with a different color ($\lambda_B = 450$ nm, $\lambda_G =$530 nm and $\lambda_R = 620$ nm). As shown in Figure S6, the imaged dots have approximately the same size, thus indicating that the image plane of the microlenses for each color is located at the same position. This discards the presence of significant chromatic aberrations in the MLA. Therefore, LCP is capable of high-FF MLA fabrication in which each individual microlens presents a high optical quality and a high photon collection efficiency.

Finally, we proved the functionality of LCP for imaging and microscopy applications. Figure 6a shows a schematic of the projection system used to characterize image formation

through a MLA. Because of the high sphericity, low surface roughness and low aberrations of the fabricated microlenses, the generated images are sharp and exhibit high contrast (Figure 6b). These results are also obtained for different microlens curvature (Figure S4b), different receiver substrates (Figure S1d) and different monochromatic light sources (Figure S7). In addition, the MLA can be used to enhance the spatial resolution of a traditional optical microscope while maintaining a large field of view. As shown in Figure 6c, an optical micrograph of a CMOS wafer acquired with a single objective lens cannot resolve the 3-µm spacing between its periodic microstructures. Instead, the MLA fabricated with LCP, and placed in close proximity to the wafer, enables to clearly resolve the structures. Combination of this strategy with sample translation[36] could result in a cost-efficient method to effectively decouple the classic tradeoff between field of view and spatial resolution of optical systems.

3. Conclusion

In conclusion, laser catapulting is a simple and rapid method for the realization of customized and high-quality MLA with a fill-factor close to 100% over a variety of substrates including flexible and curved. LCP is highly precise, accurate and capable of individual control of the microlens curvature. The fabricated MLAs are compatible with various applications including light pattern projection, high throughput microscopy, and optoelectronic systems. Importantly, because LCP uses a binary mask to shape the laser beam, the throughput of our method can be very high. Considering a beam size of 30 mm × 12 mm, a demagnification of 10 and a lens diameter of 70 µm we could transfer on a surface of 6 mm^2 an array of 1560 microlenses in a single laser pulse, which is comparable with nano-imprinting methods where thousands of micro-optical elements are fabricated in parallel in a roll-to-roll fashion.[37]

The use of high-FF microlens arrays has emerged as a valid approach for enhancing the performance of light sensitive devices. As our results demonstrate for the first time, LCP

provides an important step forward in this direction, combining ease of implementation, versatility in terms of substrates, high-throughput and high optical quality of the fabricated structures. The new technology enabled by LCP opens the door to the direct and cost-effective fabrication of MLA on top of functional devices, which can help expand the myriad of possibilities offered by microlenses in industry and science.

4. Experimental Section

Carrier substrate, donor and receiver substrate preparation: Quartz dices with size 25 mm × 25 mm and thickness of 1 mm were purchased from Solid Photon and used as carrier substrates. They were coated with a donor film consisting of a 10-µm-thick positive photoresist (S-1813, Shipley). In particular, a concentrated solution of S-1813 was deposited on the carrier by spin-coating at 1500 rpm and then subject to soft-baking on a hot-plate at 115 °C for 90 s. All the experiments of this work were performed using a 1-mm-thick PDMS (Sylgard 184, Dow Corning) as the receiver substrate unless otherwise specified. More in details, PDMS substrates were prepared by mixing curing agent and prepolymer in a 1:10 weight ratio. The mixture was degassed in a low vacuum desiccator for 1 h to remove air bubbles, poured into square-shaped (120 mm×120 mm) petri dish and finally cured at 60°C for 1 h. After that, the PDMS membrane was manually cut to obtain receiver substrates with a size of 10 mm ×10 mm. During LCP, the donor was placed directly on top of the receiver substrate (separation gap of a few microns, <5 µm). Increasing this gap causes the microdiscs to fly away[38] and, consequently, loss in the printing precision.

Laser catapulting implementation: Laser catapulting experiments were performed using a 100 Hz KrF excimer laser (Coherent-CompexPro 110). The laser emits pulses with a duration of 20 ns at an operation wavelength of 248 nm. The donor was irradiated using a mask-based projection system featuring a 0.1 numerical aperture imaging lens set at a demagnification of

8. The laser pulse on the projection mask has an energy of 160 mJ and a rectangular beam profile with flat-top distribution on the long axis (full width at half maximum or FWHM of 30 mm) and a Gaussian distribution on the short axis (FWHM of 12 mm). Each microdisc was catapulted by firing a single laser pulse at fluence levels ranging from 256 mJ/cm^2 to 1024 mJ/cm^2. Control of the laser fluence was achieved by changing the laser pulse energy using a motorized and calibrated variable attenuator. The relative position of the laser beam and the substrate was controlled by a motorized XYZ stage integrated into the laser system (Optec-MicroMaster). Thermal reflow was used to convert the printed discs into microlenses. The process was conducted in forced air ventilation oven (M250-VF, MPM Instruments) at 145°C for 30 min. A proportional-integral-derivative (PID) controller integrated into the oven enabled the temperature to be controlled with an accuracy of ±1.5°C as the reflow progressed.

Morphological and geometrical characterization: Atomic Force Microscopy (AFM) images (amplitude data) were acquired in tapping mode using an atomic force microscope (Nanowizard II, JPK Instruments) mounted on an inverted optical microscope (Axio Observer D1, Zeiss). V-shaped aluminum-coated silicon cantilevers (Bruker Nano) with a nominal spring constant of 40 N/m and pyramidal tip with a curvature radius of 10 nm were used. Morphology of both polymeric microdiscs and microlenses were investigated by means of scanning electron microscopy (JSM-6390, JEOL) at an acceleration voltage of 10 kV. To inhibit charging effects, the polymeric surfaces were previously sputter-coated with a 10-nm-thick layer of gold. The curvature of the fabricated microlenses was characterized by using a stylus profilometer (Dektak Series, Veeco Inst.). The lens ROC was calculated as the radius of the circle best fitting the microlens cross-section profile within its FWHM. ROC mean values and standard deviations were obtained by repeating the procedure over several nominally identical microlenses. Finally, precision and accuracy of the laser catapulting process were

calculated by means of optical microscopy (DM2500 M, Leica). This study was conducted over 25 and 60 nominally identical discs and lenses.

Optical characterization: Point-spread functions (PSF) of the MLA were measured with a modified confocal laser-scanning microscope (FW-100, Olympus) by serially imaging the optical sections of a collimated laser beam (λ = 488 nm) after passing through the lenses. The laser beam was reflected by a 45 degree-tilt mirror and vertically shined against the curved surfaces of the microlenses and the transmitted light is collected with a 10×/0.4 NA objective (UPlanSapo, Olympus). The focus of the objective was moved by using a mechanical stage and 20 optical planes (XY planes) with a size of 635.9 μm × 635.9 μm were imaged both above and below the microlenses focus. After a deconvolution with the PSF of the detection system (Regularized Wiener Filter, implemented in ImageJ), the lateral PSFs of each individual microlenses were obtained by post-processing the image stacks. Evaluation of the optical aberrations produced by the microlenses was carried out by means of Zernike expansion method. The light of a monochromatic plane wave (λ = 530 nm) passing thorough the microlenses was collected with 100×/0.95 NA objective (MPLANPLON, Olympus). The distorted wavefront was measured with a CCD Shack-Hartmann wavefront sensor (WFS150-5C, Thorlabs) and expressed as linear combination of the first 15 Zernike polynomials.

Imaging with MLA: Projection experiments were performed by using an upright microscope with a transmitted light path (Nikon). The light source was a cell phone screen and the image formed after the MLA was collected by a 10×/0.3NA microscope objective (Plan Fluor, Nikon). For high-resolution optical microscopy over a large field of view, a MLA with a FF of 95% was placed on top of a CMOS wafer with the curved surface of the lenses facing down. Two spacers with a thickness of 25 μm were used to control the distance between the wafer and lenses. The virtual images of the CMOS electronics were collected with a 5×/0.15NA microscope objective (Plan-Neofluar, Zeiss) and a CMOS camera (Leica).

Supporting Information
Supporting Information is available from the Wiley Online Library or from the author.

Acknowledgements
The authors thank Lara Marini for helpful discussion on DSC. S.S. and M.D. acknowledge Compagnia di San Paolo SIME 2015-0682 for financial support.

Received: ((will be filled in by the editorial staff))
Revised: ((will be filled in by the editorial staff))
Published online: ((will be filled in by the editorial staff))

References

[1] E. Wrzesniewski, S. H. Eom, W. Cao, W. T. Hammond, S. Lee, E. P. Douglas, J. Xue, *Small* **2012**, *8*, 2647.

[2] Y. Chen, M. Elshobaki, Z. Ye, J.-M. Park, M. A. Noack, K.-M. Ho, S. Chaudhary, *Phys. Chem. Chem. Phys.* **2013**, *15*, 4297.

[3] A. Orth, K. Crozier, *Opt. Express* **2012**, *20*, 13522.

[4] G. Intermite, A. McCarthy, R. E. Warburton, X. Ren, F. Villa, R. Lussana, A. J. Waddie, M. R. Taghizadeh, A. Tosi, F. Zappa, G. S. Buller, *Opt. Express* **2015**, *23*, 33777.

[5] P. Nussbaum, R. Völkel, H. P. Herzig, M. Eisner, S. Haselbeck, *Pure Appl. Opt. J. Eur. Opt. Soc. Part A* **1999**, *6*, 617.

[6] J. Aizenberg, G. Hendler, *J. Mater. Chem.* **2004**, *14*, 2066.

[7] X. Li, H. Tian, Y. Ding, J. Shao, Y. Wei, *ACS Appl. Mater. Interfaces* **2013**, *5*, 9975.

[8] Y. Peng, X. Guo, R. Liang, Y. Mou, H. Cheng, M. Chen, S. Liu, *ACS Photonics* **2017**, *4*, 2479.

[9] E. P. Chan, A. J. Crosby, *Adv. Mater.* **2006**, *18*, 3238.

[10] M. Wang, W. Yu, T. Wang, X. Han, E. Gu, X. Li, *RSC Adv.* **2015**, *5*, 35311.

[11] H.-T. Hsieh, G.-D. J. Su, *J. Micromech. Microeng.* **2010**, *20*, 35023.

[12] H. Jung, K.-H. Jeong, *ACS Appl. Mater. Interfaces* **2015**, *7*, 2160.

[13] C. Jiang, X. Li, H. Tian, C. Wang, J. Shao, Y. Ding, L. Wang, *ACS Appl. Mater. Interfaces* **2014**, *6*, 18450−18456.

[14] Y.-L. Sung, J. Jeang, C.-H. Lee, W.-C. Shih, *J. Biomed. Opt.* **2015**, *20*, 47005.

[15] H. C. Cheng, C. H. Wang, C. F. Huang, Y. K. Shen, Y. Lin, D. Y. Sheu, Y. H. Hu, *Polym. Adv. Technol.* **2010**, *21*, 632.

[16] T. Gissibl, S. Thiele, A. Herkommer, H. Giessen, *Nat. Photonics* **2016**, *10*, 554.

[17] C. Florian, S. Piazza, A. Diaspro, P. Serra, M. Duocastella, *ACS Appl. Mater. Interfaces* **2016**, *8*, 17028.

[18] S. Surdo, A. Diaspro, M. Duocastella, *Appl. Surf. Sci.* **2017**, *418*, 554.

[19] R. Ahmed, A. K. Yetisen, H. Butt, *ACS Nano* **2017**, *11*, 3155−3165.

[20] M. Duocastella, G. Vicidomini, K. Korobchevskaya, K. Pydzińska, M. Ziółek, A. Diaspro, G. de Miguel, *J. Phys. Chem. C* **2017**, *121*, 16970.

[21] J. Yong, F. Chen, Q. Yang, G. Du, H. Bian, D. Zhang, J. Si, F. Yun, X. Hou, *ACS Appl. Mater. Interfaces* **2013**, *5*, 9382.

[22] D. Nieto, M. T. Flores-Arias, G. M. O'Connor, C. Gomez-Reino, *Appl. Opt.* **2010**, *49*, 4979.

[23] C. B. Arnold, P. Serra, A. Piqué, *MRS Bull.* **2007**, *32*, 23.

[24] P. Delaporte, A. Alloncle, *Opt. Laser Technol.* **2016**, *78*, 33.

[25] A. Piqué, R. C. Y. Auyeung, H. Kim, N. A. Charipar, S. A. Mathews, *J. Phys. D. Appl. Phys.* **2016**, *49*, 223001.

[26] M. Feinaeugle, P. Gregorčič, D. J. Heath, B. Mills, R. W. Eason, *Appl. Surf. Sci.* **2017**, *396*, 1231.

[27] R. Fardel, M. Nagel, F. Nüesch, T. Lippert, A. Wokaun, *J. Phys. Chem. C* **2010**, 5617.

[28] D. P. Banks, C. Grivas, I. Zergioti, R. W. Eason, *Opt. Express* **2008**, *16*, 3249.

[29] M. S. Brown, N. T. Kattamis, C. B. Arnold, *J. Appl. Phys.* **2010**, *107*, 1.

[30] M. Duocastella, C. Florian, P. Serra, A. Diaspro, *Sci Rep.* **2015**, *5*, 16199/1.

[31] Y. M. Song, Y. Xie, V. Malyarchuk, J. Xiao, I. Jung, K. J. Choi, Z. Liu, H. Park, C. Lu, R. H. Kim, R. Li, K. B. Crozier, Y. Huang, J. A. Rogers, *Nature* **2013**, *497*, 95.

[32] J. H. Kwon, S. Choi, Y. Jeon, H. Kim, K. S. Chang, K. C. Choi, *ACS Appl. Mater. Interfaces* **2017**, *9*, 27062.

[33] M. C. Barr, J. A. Rowehl, R. R. Lunt, J. Xu, A. Wang, C. M. Boyce, S. G. Im, V. Bulović, K. K. Gleason, *Adv. Mater.* **2011**, *23*, 3500.

[34] W. Chen, R. H. W. Lam, J. Fu, *Lab Chip* **2012**, *12*, 391.

[35] S. Timoshenko, S. Woinowsky-Krieger, *Theory of Plates and Shells*, McGraw-Hill, New York, **1959**.

[36] M. Duocastella, F. Tantussi, A. Haddadpour, R. P. Zaccaria, A. Jacassi, G. Veronis, A. Diaspro, F. De Angelis, *Sci. Rep.* **2017**, *7*, 3474.

[37] C. Domínguez, N. Jost, S. Askins, M. Victoria, I. Antón, *AIP Conf. Proc.* **2017**, *1881*, 80003.

[38] S. A. Mathews, R. C. Y. Auyeung, H. Kim, N. A. Charipar, A. Piqué, *J. Appl. Phys.* **2013**, *114*, DOI: 10.1063/1.4817494.

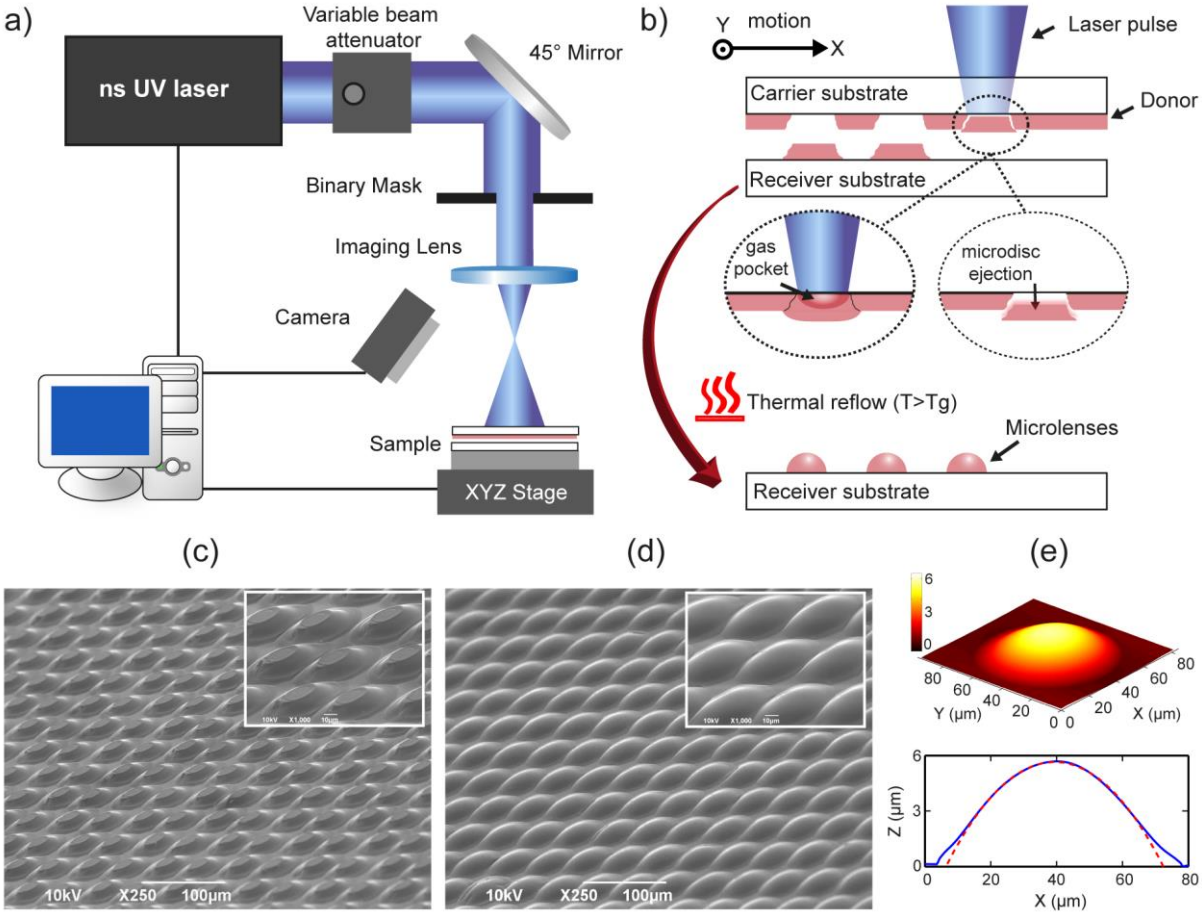

Figure 1. Working principle and practical implementation of LCP. a) Schematic of the experimental setup used for the fabrication of MLA. b) Cartoon depicting the two-step process of LCP: laser printing of solid microdiscs and thermal reflow. c) Scanning electron micrograph of a high-FF array of polymeric microdiscs and d) corresponding MLA obtained after reflow. The two insets highlight the reshaping of the microdiscs into microlenses due to the softening of the resist. e) AFM topography of a representative microlens fabricated with LCP and corresponding cross-section profile (blue line) and best fitting circle (red line).

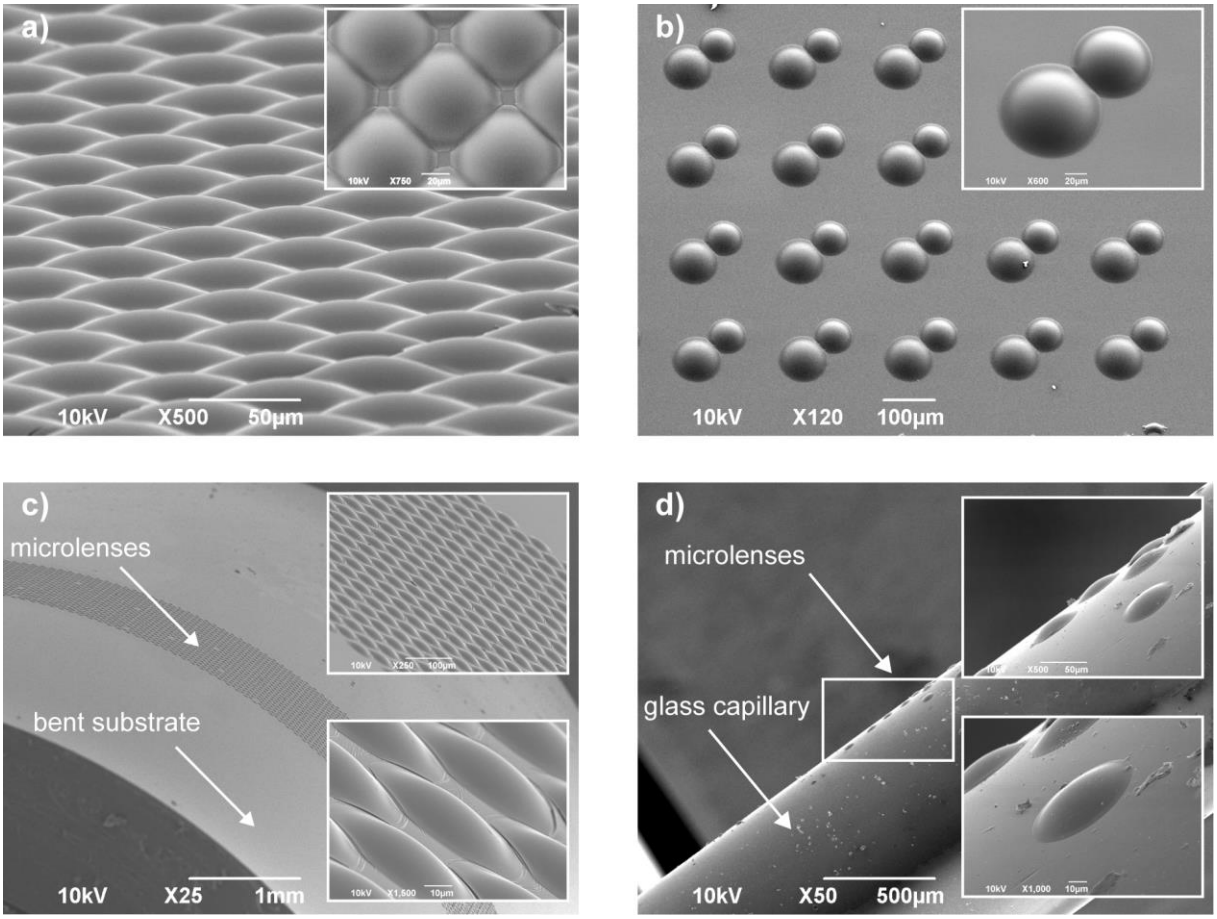

Figure 2. Scanning electron micrographs illustrating some of the fabrication possibilities offered by LCP. a) Prospective view of a MLA with a fill-factor of 99%. The inset corresponds to the top view of the array. b) Prospective view of periodically arranged dimers of microlenses with two different diameters. c) High fill-factor MLA over a flexible bent substrate. d) Polymeric microlenses over a glass capillary with a diameter of 1.22 mm.

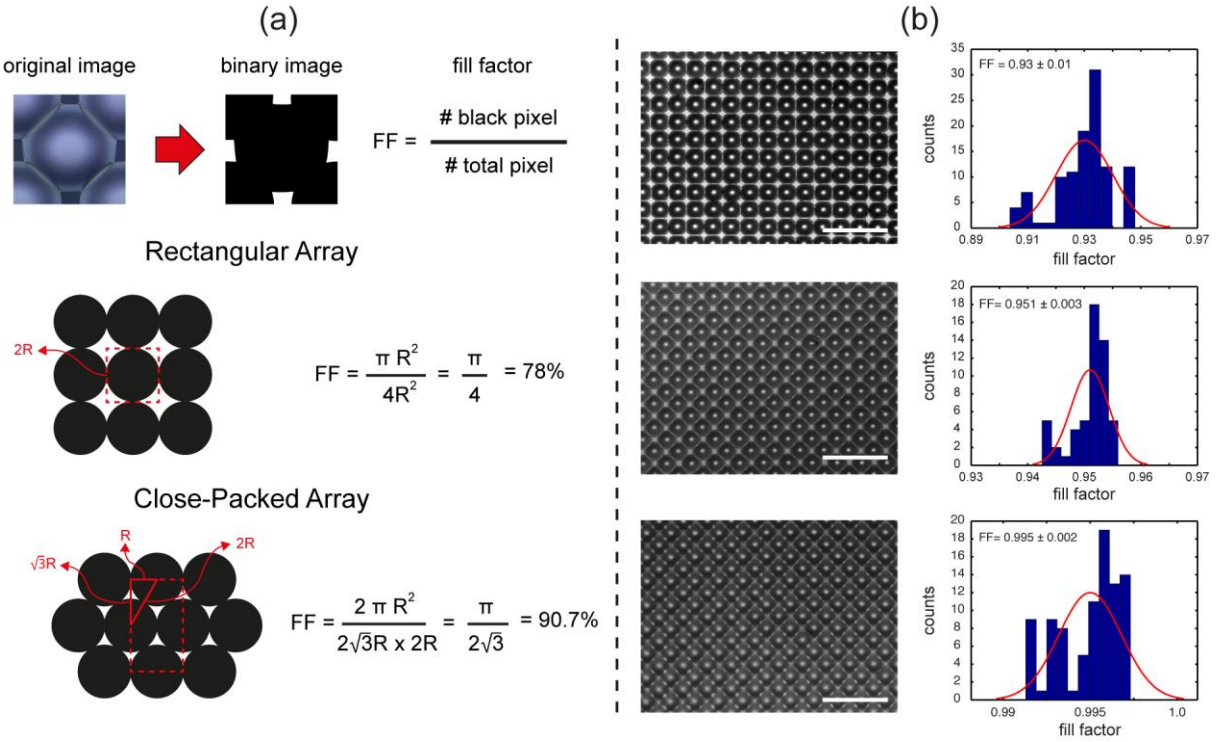

Figure 3. Study of the MLA fill-factor as a function of the geometry of the array and the microdiscs interspace distance. a) Schematic representation of the procedure used for calculating the array FF and maximum theoretical FF values of MLA with rectangular and close-packed geometries. b) Optical micrographs of MLA with, from top to bottom: rectangular geometry with 60 µm interspace distance; closed-packed geometry with 60 µm interspace distance; and closed-packed geometry with 55 µm interspace distance. The corresponding histograms reveal a fill-factor of 93%, 95%, and 99%. Scale bars are 200 µm.

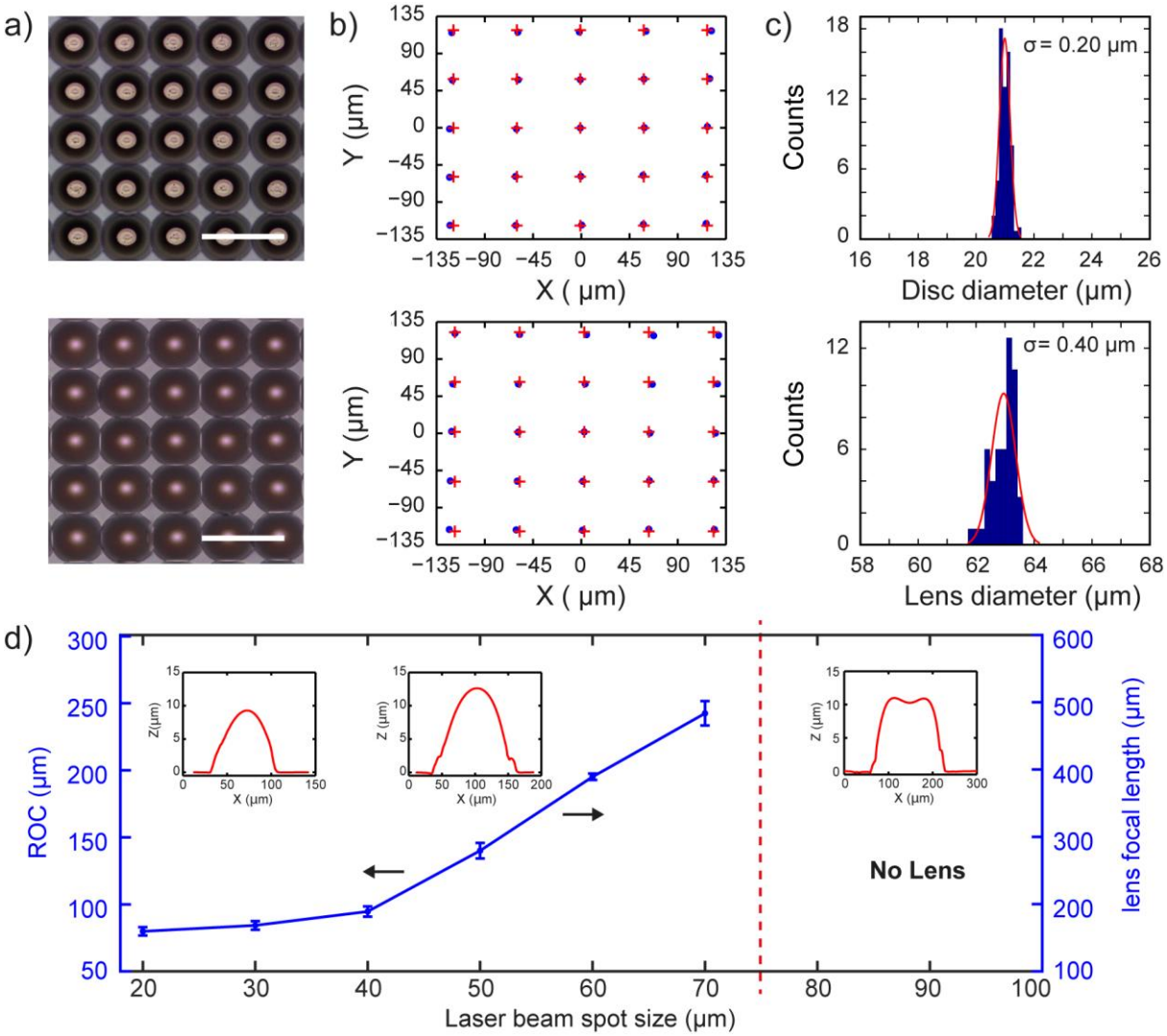

Figure 4. Technological characterization of LCP. a) Optical microscopy images of a representative portion of the microdiscs and microlens array used in the analysis. Scale bars are 100 μm. b) Experimental (blue circles) and theoretical (red crosses) centroid positions of the printed microdiscs and corresponding microlenses used to calculate the accuracy of LCP. c) Histogram of the diameter distribution of microdiscs and microlenses used to calculate the precision of LCP. d) Plot of the lens ROC (left y-axis) and focal length f_S (right y-axis) versus the laser beam spot size. The dashed line indicates the spot size above which no spherical profiles were obtained after the reflow. The insets show the cross-section profiles of microlenses obtained with a laser spot size of 20, 50 and 100 μm.

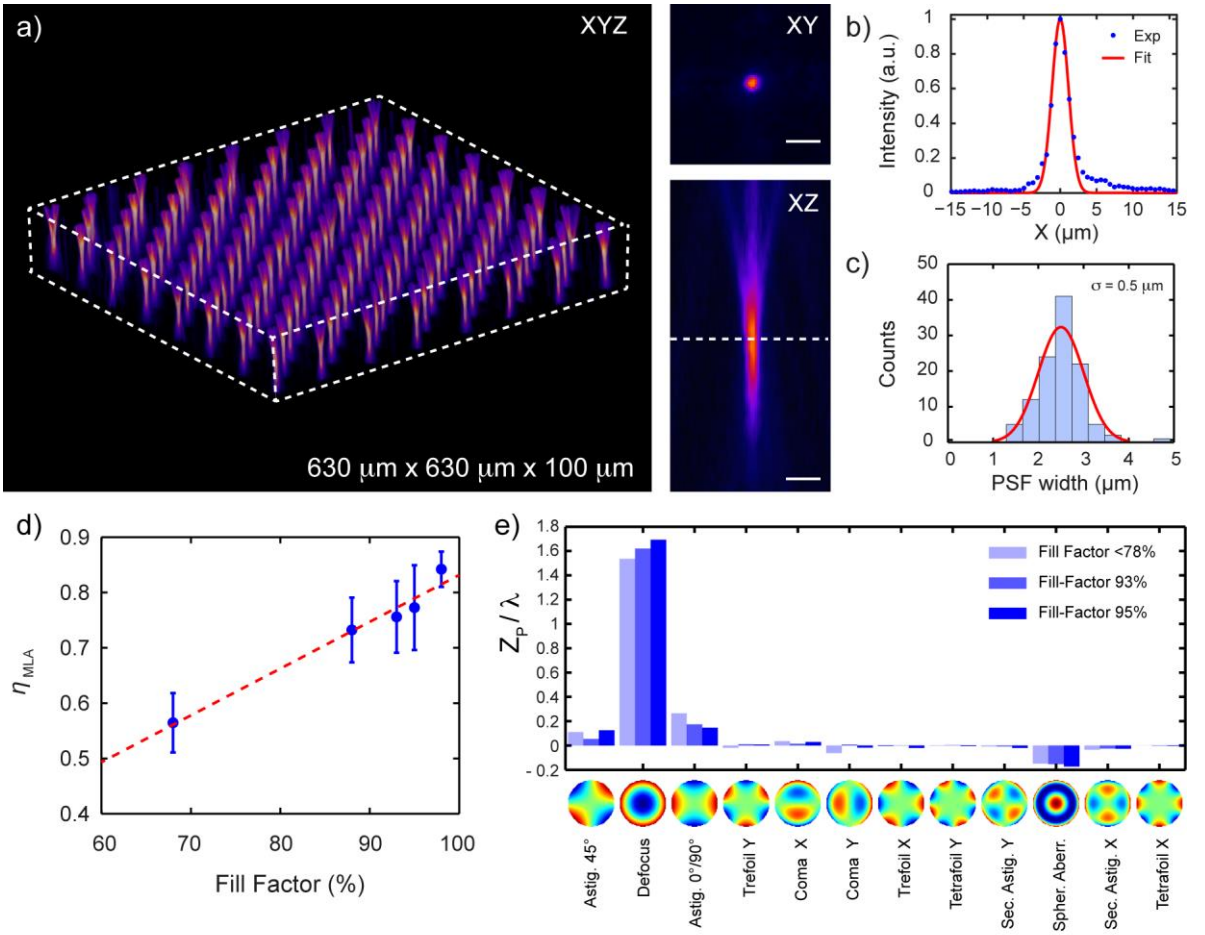

Figure 5. Optical characterization of the fabricated MLA. a) 3D reconstruction of the PSF of 100 microlenses (base diameter ~ 60 µm, height 10 µm and radius 80 µm) packed into an array with a fill-factor of ~ 99%. The maximum intensity projections on the XY and XZ planes of a representative PSF are also reported. Scale bars are 10 µm. b) Experimental (blue symbols) and Gaussian fit (red line) of the lateral PSF obtained averaging the PSFs of (a). c) Distribution of the lateral PSFs shown in (a). d) Measured (blue symbols and bars) and best line fit (dashed red line) photon collection efficiency of MLA with fill-factors from 60 to 98%. e) Zernike coefficients of to the most relevant optical aberrations of microlenses packed in arrays with different fill-factors. The FF<78% denotes the case of isolated microlenses.

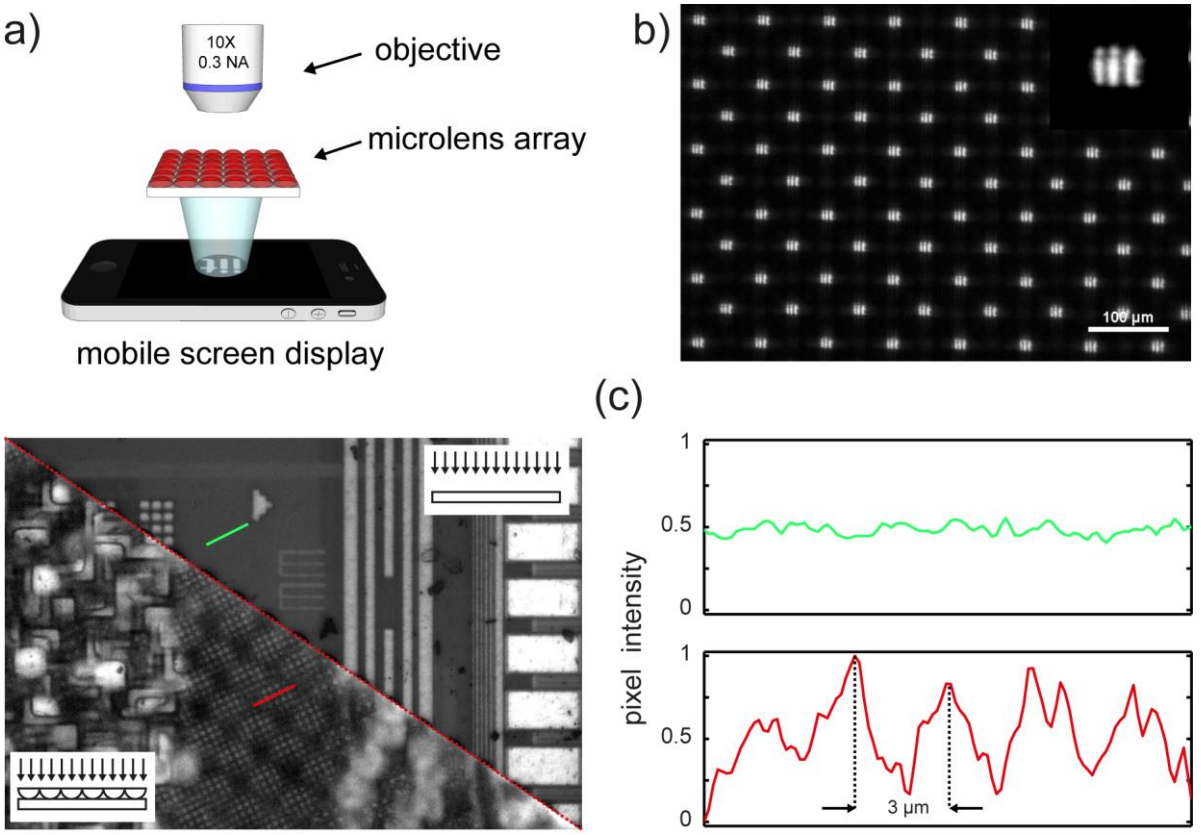

Figure 6. Functionality of the fabricated MLA. a) Scheme of the projection experiment in which a cell phone screen displays the letters "IIT", and the image formed after the MLA is collected by a microscope objective. b) Projected image after a high FF MLA. c) Large field of view (2048 µm × 1536 µm) optical microscopy images of a CMOS wafer acquired in reflection mode with (left) and without (right) the use of a MLA. The intensity profiles of the two regions of the CMOS wafer containing the same periodic microstructures highlight the gain in the resolution that is feasible with the MLA.

A novel laser additive manufacturing technique based on single-shot laser printing of polymeric discs followed by thermal reflow is presented. The method enables high-throughput fabrication of customizable microlens arrays with diffraction-limited performance and a fill-factor close to 100% directly on a variety of functional substrates including rigid, flexible and curved.

Keyword: miniaturized optics, LIFT, laser additive manufacturing, polymer patterning, resist reflow

Dr. S. Surdo, Dr. R. Carzino, Prof. A. Diaspro, Dr. M. Duocastella*
E-mail: marti.duocastella@iit.it

Single-Shot Laser Additive Manufacturing of High Fill-Factor Microlens Arrays